The following publication Y. Jia, X. Lyu, P. Xie, Z. Xu and M. Chen, "A Novel Retrospect-Inspired Regime for Microgrid Real-Time Energy Scheduling With Heterogeneous Sources," in IEEE Transactions on Smart Grid, vol. 11, no. 6, pp. 4614-4625, Nov. 2020 is available at https://doi.org/10.1109/TSG.2020.2999383.

A Novel Retrospect-inspired Regime for Microgrid Real-time Energy Scheduling with Heterogeneous Sources

Youwei Jia, *Member, IEEE*, Xue Lyu, *Member, IEEE*, Peng Xie, *Member, IEEE*, Zhao Xu, *Senior Member, IEEE*, Minghua Chen, *Senior Member, IEEE*

***Abstract*—High renewables embedded microgrid is an emerging paradigm of distributed power systems, which can locally digest intermittent generation and load demand. Due to less aggregation effect, the uncertainty issues associated with renewables and load become much more evident in small-scale microgrids, which make the energy scheduling issue even more challenging to be resolved. In this field, there generally exist two obstacles to convert the scheduling approaches into practice, which are 1) overly assumed renewable forecasting accuracy and 2) lack of effective platforms for field testing. In this paper, we firstly propose a retroactive scheduling regime in handling heterogeneous schedulable sources in small-scale microgrids, of which the decision-makings can be robust to future uncertainties. To verify the effectiveness of the proposed regime, mathematical proofs are rigorously provided for its algorithmic mechanism and performance guarantee. We then contribute a platform design to facilitate power hardware-in-the-loop experiments in a generic architecture. Experimental results demonstrate the effectiveness of the proposed regime, which suggest a high potential of its practical application.**

***Index Terms*—hardware-in-the-loop, microgrid, real-time energy scheduling, renewable energy, uncertainty**

I. Introduction

MICROGRID is an emerging paradigm of localized electrical clusters comprising of distributed energy resources (DERs) including intermittent renewables and controllable local generators. Even though the current technologies of power electronics have enabled easy integration of renewable energy sources (RES) into microgrid, its reliable and economic operation still necessitates specific energy management regimes that can effectively coordinate the internal schedulable and non-schedulable sources.

As compared to the traditional power grid, microgrid energy management is confronting with unique challenges in the following aspects. Firstly, high variability and uncertainty of RES complicate the design of energy management framework. In traditional power grid, startup and shutdown schedules of the schedulable generators are typically achieved based on proactive decision-makings through day-ahead unit commitment (UC), where RES only contributes a small portion of generation; and aggregation effect of system load make it predictable in the scheduling period of interest. In a high renewables embedded microgrid, the system scale is relatively small and the load aggregation effect becomes weak. Therefore, prediction-dependent UC may not suit the requirements of microgrid normal operation. Secondly, it is challenging to analytically assess the economic performance of a particular energy management framework in microgrid due to the stochastic nature involved in multi-timescale operational status. Deterministic evaluation through event-based analysis may be insensibly biased for microgrid [1, 2]. Moreover, economic analytics based on best/worst cases can be over optimistic/conservative.

In the literature, there generally exist three classes of methods for microgrid energy scheduling. Firstly, deterministic frameworks are directly applied in a day-ahead manner, which is similar to UC of conventional large-scale power grid. This class of methods assumes perfect forecasts for RES and load demand thus the obtained solutions may be deviated from the reality and practically infeasible [3-5]. Secondly, probabilistic approaches are adopted to deal with the prevailing uncertainties in microgrid instead of arbitrarily bypassing them. In this class, renewable generation is represented by a bunch of stochastic scenarios or probabilistic intervals. Based on this, various energy scheduling frameworks are reported in the literature by using e.g. stochastic programming [6-10], robust optimization [11-14], fuzzy logic [15] and parametric programming [16, 17] etc. Among others, the most research efforts have been endeavored in this class to design relevant energy scheduling framework. The essential research attempts are to improve the overall forecasting accuracy [18] and representability of stochastic scenarios [19]. Obviously, scenario-based stochastic frameworks rely on sufficient number of representative scenarios to reflect the possible states, of which the solving process can be computationally expensive with the increase of system scales and stochastic variables. As for robust-optimization-based methods, they normally proceed by restricting the uncertain variables within a certain set, through

Y. Jia and P Xie are with the Dept of Electrical and Electronic Engineering, Southern University of Science and Technology, Shenzhen, China (e-mail: jiayw@sustech.edu.cn)
X. Lyu is with the Dept of Electrical and Electronic Engineering, Southern University of Science and Technology, Shenzhen, China, and also with Dept. of Electrical Engineering, The Hong Kong Polytechnic University, Hong Kong
Z. Xu are with the Dept of Electrical Engineering, The Hong Kong Polytechnic University, Hong Kong
M. Chen is with the Dept of Information Engineering, The Chinese University of Hong Kong, Hong Kong

which the obtained solutions generally reflect the worst-case situations. It should be noted that both stochastic and robust optimization methods necessitate prior knowledge about the uncertainties. Hence, the resultant scheduling performance is greatly dependent on the forecasting accuracy. Thirdly, online optimization is employed to achieve real-time energy scheduling in a shorter time frame. For this class, the uncertainties are managed within a specified time window (i.e. from current to a future time slot). The typical approach to achieve online energy scheduling is based on rolling horizon strategies, which are also termed as receding horizon optimization (RHO) or model predictive control (MPC) [20-24]. In [24], comprehensive operational flexibility evaluation is provided for different multi-energy microgrids, in which MPC is utilized as an effective algorithm for short-term daily operational analyses.

Obviously, the above-mentioned methods necessarily rely on future information and instinctively give rise to proactive decision-makings for energy scheduling. That is, the overall performance would be passively influenced by the forecasting accuracy. In this regard, these methods may not be economically effective for small-scale microgrid since the prediction accuracy can be hardly guaranteed in such an environment with high intermittency and variability. Theoretically, "perfect dispatch (PD)" solutions can be obtained by given full knowledge of the future conditions, where direct-optimization in retrospect spanning the whole horizon of interest is applied [25]. Distinguished from the proactive energy scheduling, this paper is aimed to investigate the retroactive process and endeavor to answer a general question—how to leverage the retroactive insights in designing close-to-perfect energy scheduling strategies.

In recent years, several online scheduling approaches have been reported in the literature, which are dependent on zero or little forecasting information. As the pioneering work, a competitive online scheduling algorithm (which is named as CHASE) is firstly proposed in [26, 27], in which competitive ratio[1] is employed to evaluate the overall performance of the algorithm. Theoretically, these exists performance guarantee that the competitive ratio is proven to be no greater than 3. In [28], regret minimization is deployed (instead of competitive ratio) to achieve online scheduling based on a modified ADMM algorithm, which provides less conservative scheduling solutions than the robust optimization-based approach. Undoubtedly, such prediction-independent frameworks are of high interest for small-scale microgrid application. However, a meaningful question from practical aspect still remains open—to which extent is the obtained scheduling solution in practice close to perfect dispatch.

Even though many research works in microgrid energy scheduling have been reported in the existing literature, most of them are only compared and verified through computer simulations without being tested experimentally. Admittedly, there always exist a gap between theoretical proposals and practical implementation. In both industry and academia, it has been widely accepted that hardware-in-the-loop (HIL) experiments can offer viable routes to developmental testing at scales [29]. Thus far, several HIL microgrid testbeds have been reported whereas they mainly focus on energy management for RES and battery system in grid-connected/islanded modes(e.g. [30]), control functions of microgrid components (e.g. [31, 32]), and system monitoring & measurements (e.g. [33]). At the system level, creating a scalable integrated HIL platform for microgrid real-time scheduling is of vital importance yet challenging due to the factors that 1) uncertainties should be suitably modeled in the HIL system; 2) an efficient communication system should be established to govern the information flow among all system components; 3) non- / schedulable generators should be emulated in an effective way; 4) a high-performance computation engine is imperative to harness necessary optimization tasks; and 4) the whole HIL platform design should globally consider the synergy and interaction among optimization, communication and hardware control.

In this paper, we firstly tackle the real-time energy scheduling problem in presence of high uncertainty by investigating CHASE inspired retroactive regime. To bridge the gap for practical application, a power HIL (PHIL) microgrid platform has been developed, through which the extensive case studies are carried out and the effectiveness of the proposed regime is verified.

The main contributions of this paper are threefold:

- A retroactive energy scheduling regime based on *h*CHASE in small-scale microgrid is newly developed. The proposed generalized *h*CHASE has distinctive merits on i) heterogeneity handling for various kinds of schedulable units in microgrids; ii) effective performance guarantee in presence of different levels of forecasting accuracy; and iii) high extensibility and scalability for practical application.
- We newly derive the theoretical limit of the competitive ratio for *h*CHASE with rigorous mathematical proofs. Through extensive evaluations by using real-world data, it has been revealed that the upper bound for typical cases are generally below 2. Such results possess more realistic significance.
- We contribute a design of power hardware-in-the-loop microgrid platform, which consists of advanced modules for measurement & monitoring, computation, data acquisition and real-time control. This platform is capable of emulating time-varying generation and loading profiles. MPC method and the proposed *h*CHASE based regime are explicitly tested and compared on this platform, through which the effectiveness of *h*CHASE is duly verified.

[1] Competitive ratio is defined as the ratio between sub-optimal cost obtained by a particular energy scheduling approach and optimal cost obtained by perfect dispatch. i.e.

$$CR = \frac{cost(\text{sub-optimal})}{cost(\text{optimal})}$$

II. Retroactive Regime for Real-time Energy Scheduling

A. CHASE-based Operating Regime and Practical Extensions

In managing the unavoidable uncertainties in microgrid operation, CHASE algorithm is firstly proposed in [26], which provides a promising solution to tracing the optimal on/off status of schedulable units in a heuristic way. The essential idea behind CHASE is to leverage the retroactive insights of perfect dispatch solution. Admittedly, CHASE algorithm lays a significant foundation for online decision-makings of energy scheduling based on deterministic regime, of which the competitive ratio is proven to be **3**. However, this prediction-oblivious algorithm necessarily relies on the following assumptions, which make it hardly be implemented in practice. The concerned theoretical assumptions include: 1) the operational parameters of all schedulable units are homogeneously assigned, including the power capacity, start-up, sunk and incremental cost, etc.; and 2) conceivable improvements on the scheduling solutions can be achieved by given perfect forecasting accuracy of renewable generation and load demand in a certain lookahead time window.

In reality, the schedulable units in a microgrid are generally various in terms of power capacity and operational cost. In this sense, homogeneous settings for all generators can make the constructed models less extensible for real-case implementation, especially for the case with multiple heterogeneous generators. Meanwhile, the competitive ratio of **3** reflects the worst case indicating complete mismatch between CHASE solutions and the retrospect of perfect dispatch. This however is insufficient to demonstrate the effectiveness of CHASE in leading to economic energy scheduling.

In consideration of future forecasting information, Ref [34] restudies this online energy scheduling problem for grid-connected microgrid with the proposals of *r*CHASE and *i*CHASE. Specifically, *r*CHASE makes algorithmic decisions based on the probability distribution that depicts the randomness of future information (i.e. renewable generation and load demand). *i*CHASE is further extended upon *r*CHASE by considering possible prediction intervals. Such extensions become much more realistic as compared to the original algorithm, since the uncertainties involved in future information is properly taken into account. In addition, the competitive ratio of *r*CHASE and *i*CHASE is proven to be **2.128** at most.

As reported in our previous work [35], the competitive ratio of retroactive regime is numerically evaluated based on realistic operation data in Belgium. Through extensive case studies, it has been revealed that the averaging competitive ratio of retroactive regime is mostly less than 1.1. It can be seen that there exists a gap between the numerical results and theoretical upper bound (i.e. the proven performance guarantee of basic CHASE and its practical extensions).

Based on the above-mentioned analysis, this paper is aimed to overcome the present limitations and proposes an enhanced and generalized algorithm named as *h*CHASE. As compared to the previous works, *h*CHASE is advantageous over the original algorithm and its prediction-aided versions in the following aspects — i) heterogeneity of schedulable units is properly handled; ii) different levels of forecasting accuracy is considered to evaluate its performance guarantee; and iii) it features high extensibility and scalability for practical application.

B. Problem Description of Energy Scheduling in Microgrid

In this paper, the energy scheduling problem of interest is modeled as a real-time rolling horizon optimization problem (RHOP) in grid-connected mode. A typical one-bus microgrid architecture is shown in Fig. 1, which consists of multiple schedulable generation units with heterogeneous features, renewable generators and load demand. The heterogeneity on generation capacity and operational cost (including start-up, sunk and incremental cost) is fully considered in our study. A detailed discussion on start-up cost of local generators can be referred to [36]. Since the concerned microgrid in our study operates in a grid-connected mode, the power exchange between the microgrid and the main grid can timely complement the instant power imbalance. The exchange amount is subject to real-time electricity price.

It should be noted that formulated RHOP model is still applicable to energy scheduling in microgrid stand-alone mode, where energy storage system serves as a finite grid-forming unit, and the battery degradation cost should be considered. Since the focus of this paper is on the across-time-coupled scheduling problem with uncertainties, hence one-bus microgrid in grid-connected mode can adequately reflect the concerned problem nature.

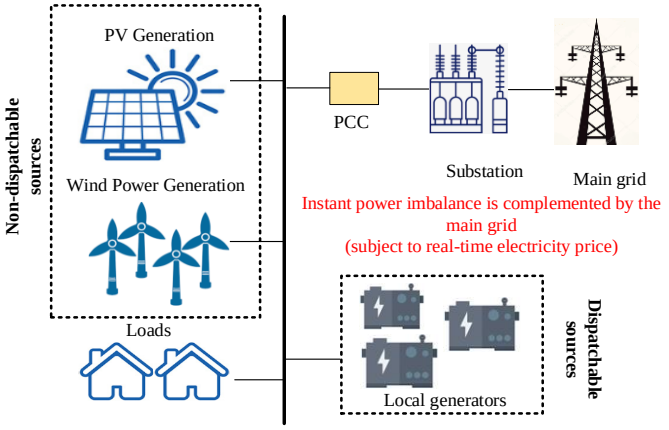

Fig.1 System model of grid-connected microgrid

Specifically, the RHOP is formulated in the following.

$$\min_{y_i\in\{0,1\},P_i(t)\in\mathbb{R}^+} \sum_{t=t_1}^{t^*}\sum_{i=1}^{N} cost(y_i(t),P_i(t)) + \lambda(t)P_{grid}(t) \tag{1}$$

$$\textbf{s.t.} \quad P_i^{\min} \le P_i(t) \le P_i^{\max} \tag{2}$$

$$\sum_{i=1}^{N} P_i(t) + P_{grid}(t) = P_{load}(t) \tag{3}$$

$$P_i(t+1) - P_i(t) \le P_i^{up} \tag{4}$$

$$P_i(t) - P_i(t-1) \le P_i^{down} \tag{5}$$

$$y_i(\tau) \ge 1_{\{y_i(t)>y_i(t-1)\}},\ t+1 \le \tau \le t+T_i^{on}-1 \tag{6}$$

$$y_i(\tau) \le 1-1_{\{y_i(t)<y_i(t-1)\}},\ t+1 \le \tau \le t+T_i^{off}-1 \tag{7}$$

where c_i^{incr}, c_i^{sunk} and c_i^{start} denote the incremental, sunk and start-up cost of local generator *i*, respectively; $\lambda(t)$ denotes the spot price of purchased electricity from the main grid at time slot *t*; $\mathbb{1}\{\cdot\}$ denotes the indicator function; T_i^{on} (T_i^{off}) represents the minimum on- (off-) time of *i*-th local generator; the total number of local generators is *N*; $P_{grid}(t)$ denotes the exchange power from the microgrid to the main grid; the cost function is approximated in a linear form and expressed in Eq (8):

$$cost(y_i(t), P_i(t)) = c_i^{incr} P_i(t) y_i(t) + c_i^{sunk} y_i(t) + c_i^{start} [y_i(t) - y_i(t-1)]^+ \quad (8)$$

where $P_i(t)$ and $y_i(t)$ are the decision variables denoting the power output and on/off status of the *i*-th generator, respectively.

The formulated RHOP concerns the cost in a rolling time window. The lookahead steps contains $\sigma = t^* - t_1$ time slots (t_1 is the current time slot, t^* is the last time slot in the lookahead window). In this RHOP model, (2) and (3) represent the power output constraint of *i*-th generator and power balancing constraint of the whole system, respectively. (4) and (5) represent the ramping up and down constraints of *i*-th generator, respectively. (6) and (7) represent the minimum on- and off-time constraints of the *i*-th generator.

Remark: All decision variables of RHOP is across time coupled. Such formulation is generally considered to be NP-complete. Even though this optimization problem can be readily handled by the classical MPC method, the obtained solutions become sub-optimal and can be greatly influenced by the forecasting accuracy (Interested reader can refer to the extensive numerical results in [35]).

C. hCHASE for General Case of Heterogeneous Generators

Instead of directly applying MPC to the concerned RHOP, we propose a generalized *h*CHASE algorithm to suffice the operating scenarios with multiple heterogeneous generators in a heuristic way, where a certain degree of forecasting information is taken into account.

Essentially, *h*CHASE is devised to optimally allocate suitable generation units to supply a certain amount of load. That is, the complete RHOP is decomposed into *N* sub-RHOPs, which is consistent with the total number of local generators.

In the following definition, RHOP decomposition is defined as a optimal load partitioning problem.

Definition 1: given *N* local schedulable generators in a microgrid, the corresponding generation capacity is $\{P_1^{\max}, P_2^{\max}, ..., P_N^{\max}\}$. Accordingly, the load demand is partitioned into *N* layers with the order $\{\beta_1, \beta_2, ..., \beta_N\}$ (as shown in Fig.2). Each layer is specified as,

$$P_{load}^{ly-n}(t) = \min\{P_{\beta_n}^{\max}, P_{load}(t) - \sum_{j=1}^{n-1} P_{load}^{ly-j}(t)\}, n \in [1, N] \quad (9)$$

Based on Definition 1, $\{\alpha_1, \alpha_2, ..., \alpha_N\}$ becomes an optimal order for load partitioning if and only if the follow inequality is satisfied.

$$cost[(y_{\alpha_i}, P_{\alpha_i})_{i=1}^N, P_{grid}] \le cost[(y_{\beta_i}, P_{\beta_i})_{i=1}^N, P_{grid}] \quad (10)$$

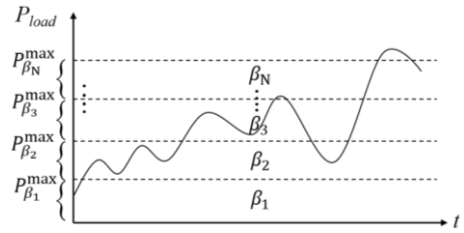

Fig.2 Schematic diagram of load partitioning

To ensure the optimality of the decomposition complies with the whole RHOP, this paper provides a complete proof for the inequality relationship of (10). The mathematical details are presented in Theorem 1.

Theorem 1: suppose $(y_{\alpha_n}, P_{\alpha_n}, P_{grid}^{\alpha_n})$ is an optimal solution for the *n*-th sub-problem, then $[(y_{\alpha_n}^\dagger, P_{\alpha_n}^\dagger)_{n=1}^N, P_{grid}^\dagger]$ is the optimal solution for the whole RHOP, where

$$y_{\alpha_n}^\dagger(t) = y_{\alpha_n}(t),\ P_{\alpha_n}^\dagger(t) = P_{\alpha_n}(t),\ P_{grid}^\dagger(t) = \sum_{i=1}^{N} P_{grid}^{\alpha_n}(t),\ n \in [1, N] \quad (11)$$

Under the condition that (10) is strictly satisfied, theorem 1 can be rigorously confirmed. The mathematical proof is provided in Section III-A.

Theorem 1 lays out significant foundation in designing *h*CHASE, through which the on/off decisions of local generators can be individually made based on the original CHASE algorithm in a deterministic manner. The proposed retroactive regime based on *h*CHASE is shown in Fig. 3.

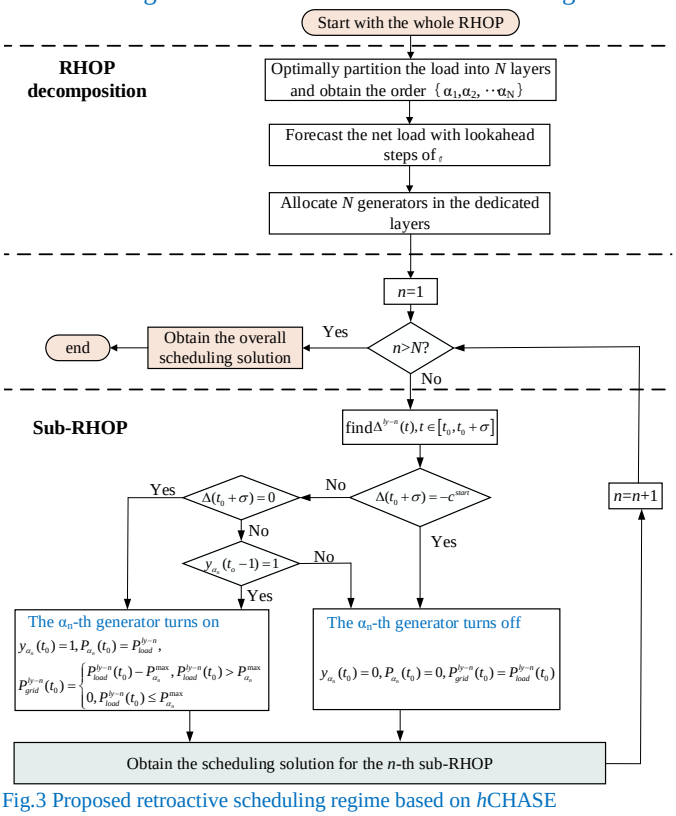

Fig.3 Proposed retroactive scheduling regime based on *h*CHASE

As illustrated in Fig. 3, the proposed *h*CHASE comprises of two essential components:

Firstly, the original RHOP is decomposed by optimally partitioning the load demand into *N* layers. The load partitioning is achieved based on a rough day-ahead forecast.

Through extensive numerical studies on realistic operational data, it has been shown that such a rough forecast is sufficient to reflect the general trend of the load demand of a whole day, and thus it can lead to effective load partitioning solutions [35]. This partitioning problem is mathematically formulated as follows:the cost regret (or termed as opportunity cost) is iteratively calculated according to (14).

$$\delta_{\alpha_n}(t) = cost[y_{\alpha_n}(t)=0, P_{\alpha_n}(t)=0, P_{grid}^{ly-n}] - cost[y_{\alpha_n}(t)=1, P_{\alpha_n}(t), P_{grid}^{ly-n}=0] \quad (14)$$

Cumulative cost regret is an essential indicator for decision-makings (as referred to [26]), which is expressed as:

$$\Delta^{ly-n}(t) = \min\{0, \max\{-c_{\alpha_n}^{start}, \Delta^{ly-n}(t-1) + \delta_{\alpha_n}(t)\}\} \quad (15)$$

The performance guarantee of the proposed *h*CHASE is given in Theorem 2.

Theorem 2: for each sub-RHOP with certain degree of forecasting error, the competitive ratio of *h*CHASE satisfies:

$$CR_{hCHSASE} \le \frac{\sum_{i=1}^{N} CR_{\max}^{i} \cdot cost_i(optimal)}{\sum_{i=1}^{N} cost_i(optimal)} \quad (16)$$

where CR^i is the competitive ratio for each sub-RHOP. In particular,

$$CR^i \le 1 + \frac{4c_{\alpha_i}^{start} + \varepsilon P_{load}^{\min}(\lambda_{\min}^{up} - \lambda_{\max}^{dw})_{\alpha_i} + 4(\sigma+1)c_{\alpha_i}^{sunk}}{2c_{\alpha_i}^{start}(1+\gamma)} \quad (17)$$

where ε is *prediction constant* (in this paper, the relation between forecasting accuracy and lookahead time window is assumed to be linear. Detailed model can be referred to Section V-B); and

$$\gamma_{\alpha_i} = \frac{P_{load}^{\max} c_{\alpha_i}^{incr} + c_{\alpha_i}^{sunk}}{P_{load}^{\max}(\lambda_{\max} - c_{\alpha_i}^{incr}) - c_{\alpha_i}^{sunk}} \quad (18)$$

$$\lambda_{\min}^{up} : \min\{\lambda(t) \mid \lambda(t) \ge c_{\alpha_i}^{incr}\} \quad (19)$$

$$\lambda_{\max}^{dw} : \max\{\lambda(t) \mid \lambda(t) < c_{\alpha_i}^{incr}\} \quad (20)$$

The proof of Theorem 2 is provided in Section III-B.

Remark: Being consistent with CHASE, forecasting information is not a necessary input for *h*CHASE, which however can increase the overall scheduling performance to a great extent.

III. Mathematical Validation of *h*CHASE

In this section, the mathematical proof for the effectiveness of RHOP decomposition and performance guarantee of *h*CHASE will be provided in detail.

A. Proof of RHOP Decomposition (Theorem 1)

Suppose that $[(\tilde{y}_i, \tilde{P}_i)_{i=1}^N, \tilde{P}_{grid}]$ is an optimal solution for the RHOP. We construct a new feasible solution based on $[(\tilde{y}_i, \tilde{P}_i)_{i=1}^N, \tilde{P}_{grid}]$ as: $[(\hat{y}_i, \hat{P}_i)_{i=1}^N, \hat{P}_{grid}]$.

Since (y_i, P_i, P_{grid}^i) is an optimal solution for each sub-problem, so $cost(\hat{y}_i) \ge cost(y_i)$ (21)

We define $[(\hat{y}_i, \hat{P}_i)_{i=1}^N, \hat{P}_{grid}]$ as:

$$\hat{y}_{\alpha_n}(t) = \begin{cases} 1, if\ \ \hat{P}_{\alpha_1}(t) > 0 \\ 0, otherwise \end{cases} \quad (22)$$

where $\hat{P}_{\alpha_1}(t) = \min\{P_{\alpha_1}^{\max}, \sum_{i=1}^{N} \tilde{P}_i(t)\}$ (23)

$$\hat{P}_{\alpha_n}(t) = \min\{P_{\alpha_n}^{\max}, \sum_{i=1}^{N} \tilde{P}_i(t) - \sum_{i=1}^{n-1} \tilde{P}_i(t)\} \quad (24)$$

Furthermore, one can obtain

$$\hat{P}_{grid}^{\alpha_n} = [P_{load}^n(t) - \hat{P}_{\alpha_n}(t)]^+ \quad (25)$$

It is straightforward to obtain that

$$\sum_{i=1}^{N} \hat{y}_{\alpha_i}(t) = \sum_{i=1}^{N} \hat{y}_i^{\dagger}(t) \ \text{ and } \ \sum_{i=1}^{N} \tilde{P}_i(t) = \sum_{i=1}^{N} \hat{P}_{\alpha_n}(t)$$

Finally, by Lemmas 1 and 2, one can obtain that

$$cost[(\tilde{y}_i, \tilde{P}_i)_{i=1}^N, \tilde{P}_{grid}] \ge cost[(\hat{y}_i, \hat{P}_i)_{i=1}^N, \hat{P}_{grid}] \ge \sum_{n=1}^{N} cost(\hat{y}_{\alpha_n}, \hat{P}_{\alpha_n}, \hat{P}_{\alpha_n})$$

Therefore, $[(y_{\alpha_n}^{\dagger}, P_{\alpha_n}^{\dagger})_{n=1}^N, P_{grid}^{\dagger}]$ is the optimal solution to the RHOP.

Lemma 1

$$\sum_{i=1}^{N} \hat{P}_{grid}^i(t) \le \sum_{i=1}^{N} \tilde{P}_{grid}^i(t) = \tilde{P}_{grid}(t) \quad (26)$$

Proof

Since $P_{load}^n(t) \ge \hat{P}_{\alpha_n}(t)$, thus

$$\sum_{i=1}^{N} \hat{P}_{grid}^i(t) = \sum_{n=1}^{N} \hat{P}_{grid}^{\alpha_n}(t) = \sum_{n=1}^{N} [P_{load}^n(t) - \hat{P}_{\alpha_n}(t)]^+$$
$$= P_{load} - \sum_{n=1}^{N} \hat{P}_{\alpha_n}(t) = P_{load} - \sum_{i=1}^{N} \hat{P}_i(t) \le \sum_{i=1}^{N} \tilde{P}_{grid}^i(t) = \tilde{P}_{grid}^i(t)$$

Lemma 2

$$\text{cost}[(\hat{y}_n, \hat{P}_n)_{n=1}^N] \le \text{cost}[(\tilde{y}_i, \tilde{P}_i)_{i=1}^N] \quad (27)$$

Proof

Since $\{\alpha_n\}_{n=1}^N$ corresponds to an optimal load partitioning solution, thus

$$cost[(y_{\alpha_n}, P_{\alpha_n})_{n=1}^N, P_{grid}]_{\min} \le cost[(y_{\beta_n}, P_{\beta_n})_{n=1}^N, P_{grid}]_{\min} \quad (28)$$

According to (22)-(24), $\sum_{i=1}^{N} P_i(t)$ is partitioned into N layers in the same way as the load. Besides, each layer is dedicated a generation unit corresponding to the optimal order $\{\alpha_n\}_{n=1}^N$. Thus,

$$\text{cost}[(\hat{y}_{\alpha_n}(t), \hat{P}_{\alpha_n}(t))_{n=1}^N]$$
$$= \sum_{n=1}^{N} (\hat{P}_{\alpha_n}(t) \cdot c_{\alpha_n}^{incr} + c_{\alpha_n}^{sunk}) + \sum_{n=1}^{N} (\hat{y}_{\alpha_n}(t) - \hat{y}_{\alpha_n}(t-1))^+ \cdot c_{\alpha_n}^{start}$$
$$= \sum_{n=1}^{N} (\hat{P}_{\alpha_n}(t) \cdot c_{\alpha_n}^{incr} + c_{\alpha_n}^{sunk}) + [\sum_{n=1}^{N} \hat{y}_{\alpha_n}(t) - \sum_{n=1}^{N} \hat{y}_{\alpha_n}(t-1)]^+ \cdot c_{\alpha_n}^{start}$$
$$= \sum_{n=1}^{N} (P_{\alpha_n}(t) \cdot c_{\alpha_n}^{incr} + c_{\alpha_n}^{sunk}) + [\sum_{n=1}^{N} y_{\alpha_n}(t) - \sum_{n=1}^{N} y_{\alpha_n}(t-1)]^+ \cdot c_{\alpha_n}^{start}$$
$$\le \sum_{n=1}^{N} (P_{\alpha_n}(t) \cdot c_{\alpha_n}^{incr} + c_{\alpha_n}^{sunk}) + \left[\sum_{n=1}^{N} \left[y_{\alpha_n}(t) - y_{\alpha_n}(t-1)\right]^+\right] \cdot c_{\alpha_n}^{start}$$
$$= cost[(y_{\alpha_n}(t), P_{\alpha_n}(t))_{n=1}^N]_{\min}$$

Since (28), one can obtain

$$\text{cost}[(y_{\alpha_n}(t), P_{\alpha_n}(t))_{n=1}^N]_{\min} \le \text{cost}[(\tilde{y}_i(t), \tilde{P}_i(t))_{i=1}^N]$$

Thus,

$$\text{cost}[(\hat{y}_n, \hat{P}_n)_{n=1}^N] \le \text{cost}[(\tilde{y}_i, \tilde{P}_i)_{i=1}^N]$$

It completes the proof.

B. Proof of Competitive Ratio for sub-RHOP (Theorem 2)

Assumed that the relation between net load forecasting error and σ is linear, thus,

$$\eta(t+\sigma) \le \frac{P^{*}_{load}(t+\sigma)}{P_{load}(t+\sigma)} \le 2-\eta(t+\sigma) \tag{29}$$

where $d \in [0,1]$ is the forecasting accuracy, and

$$\eta(t+\sigma) = \sigma(d-1)+1 \tag{30}$$

In a sub-RHOP, critical segments are classified into 4 types as the same with [26]. We denote the set of indices of dispatching segments of type-k by $\mathcal{T}_k$. Define the number of type-k dispatching segments as $m_k = |\mathcal{T}_k|$. It is straightforward that $m_1 = m_2 + m_3$.

For type-0, $y^{PD}(t) = y^{hCHASE}(t) = 0$. Hence,

$$\text{cost}^{ty-0}_{PD}[y(t),P(t),P_{grid}(t)] = \text{cost}^{ty-0}_{PD}[y(t),P(t),P_{grid}(t)] \tag{31}$$

For type-1, one can obtain $\Delta(T^c_s) = -c^{start}$ and $\Delta(\tilde{T}^c_s) = 0$. We look into the segment $\tilde{T}^c_s - \phi + 1 < T^c_{s+1}$. It is noted that

$$y^{hCHASE}(t) = \begin{cases} 0, t \in [T^c_s + 1, \tilde{T}^c_s - \phi] \\ 1, t \in [T^c_s - \phi + 1, \tilde{T}^c_{s+1}] \end{cases} \tag{32}$$

Based on the definition of type-1, one can obtain:

$$\begin{aligned} &\sum_{t=T^c_s+1}^{\tilde{T}^c_s-1} [\text{cost}(y(t)=0,P(t)=0,P_{grid}(t)) - \text{cost}(y(t)=1,P(t),P_{grid}(t)=0)] \\ &\quad + c^{start} - c^{start} \\ &= \sum_{t=T^c_s+1}^{\tilde{T}^c_s-\phi-1} \delta(t) = \Delta(\tilde{T}^c_s - \phi - 1) - \Delta(T^c_s) = \Delta(\tilde{T}^c_s - \phi - 1) + c^{start} \end{aligned} \tag{33}$$

Thus,

$$\text{cost}^{ty-1}_{hCHASE} \le \text{cost}^{ty-0}_{PD} + m_1 c^{start} + \sum_{s=1}^{m_1} \Delta(\tilde{T}^c_s - \phi - 1) \tag{34}$$

Recall Algorithm 1, one obtains,

$$\Delta(\tilde{T}^c_s - \phi - 1) + \sum_{t=\tilde{T}^c_s-\phi}^{\tilde{T}^c_s-\phi+\sigma} \delta^{*}(t) = 0 \tag{35}$$

Thus,

$$\begin{aligned} &\Delta(\tilde{T}^c_s - \phi - 1) = -\sum_{t=\tilde{T}^c_s-\phi}^{\tilde{T}^c_s-\phi+\sigma} \delta^{*}(t) = -\sum_{t=\tilde{T}^c_s-\phi}^{\tilde{T}^c_s-\phi+\sigma} \{[\lambda(t) - c^{incr}]P_{load}(t)\cdot\eta(t) - c^{sunk}\} \\ &\le -\sum_{t=\tilde{T}^c_s-\phi}^{\tilde{T}^c_s-\phi+\sigma} [(\lambda^{up}_{\min} - c^{incr})]P^{\min}_{load}\cdot\eta(t) - c^{sunk}] \\ &\le (\frac{\sigma(\sigma-1)}{2} - \frac{(\sigma+1)\sigma\cdot d}{2} - 1)\cdot(\lambda^{up}_{\min} - c^{incr})P^{\min}_{load} + (\sigma+1)c^{sunk} \end{aligned} \tag{36}$$

For type-2 and type-3, we can derive similarly for k=2 and k=3.

$$\text{cost}^{ty-k}_{hCHASE} \le \text{cost}^{ty-k}_{PD} - \sum_{s=1}^{m_k} \Delta(\tilde{T}^c_s - \phi - 1) \tag{37}$$

where $\Delta(\tilde{T}^c_s - \phi - 1) + \sum_{t=\tilde{T}^c_s-\phi}^{\tilde{T}^c_s-\phi+\sigma} \delta^{*}(t) = -c^{start}$, hence

$$\begin{aligned} -\Delta(\tilde{T}^c_s - \phi - 1) \le c^{start} + \{(c^{incr} - \lambda^{dw}_{\max})P^{\min}_{load}(\frac{\sigma(\sigma-1)}{2} - \frac{(d+\sigma d)\sigma}{2} - 1) \\ + (\sigma+1)c^{sunk}\} \end{aligned}$$

Recall that $m_1 = m_2 + m_3$. Based on (36) and (37), one obtains,

$$\frac{\text{cost}_{hCHASE}}{\text{cost}_{PD}} = \frac{\sum_{k=0}^{3} \text{cost}^{ty-k}_{hCHASE}}{\text{cost}_{PD}} \tag{38}$$

$$\begin{aligned} &\le \frac{2m_1 c^{start} + m_1(\frac{\sigma^2-\sigma-\sigma^2 d-\sigma d-2}{2})P^{\min}_{load}(\lambda^{up}_{\min} - \lambda^{dw}_{\max}) + 2m_1(\sigma+1)c^{sunk}}{\text{cost}_{PD}} + 1 \\ &\le 1 + \frac{2m_1 c^{start} + m_1(\frac{\sigma^2-\sigma-\sigma^2 d-\sigma d-2}{2})P^{\min}_{load}(\lambda^{up}_{\min} - \lambda^{dw}_{\max}) + 2m_1(\sigma+1)c^{sunk}}{\text{cost}^{ty-1}_{PD}} \end{aligned} \tag{39}$$

According to Lemma 4 in [26],

$$\text{cost}^{ty-1}_{PD} \ge m_1(c^{start} + c^{start}\frac{P^{\max}_{load}\cdot c^{incr} + c^{sunk}}{P^{\max}_{load}(\lambda_{\max} - c^{incr}) - c^{sunk}}) \tag{40}$$

Substitute (40) to (39), (38) becomes

$$\frac{\text{cost}_{hCHASE}}{\text{cost}_{PD}} \le 1 + \frac{4c^{start} + \varepsilon P^{\min}_{load}(\lambda^{up}_{\min} - \lambda^{dw}_{\max}) + 4(\sigma+1)c^{sunk}}{2c^{start}(1+\gamma)}$$

where

$$\varepsilon = \sigma^2 - \sigma - \sigma^2 d - \sigma d - 2 \tag{41}$$

Therefore, it completes the proof.

IV. Power Hardware-in-the-loop Platform

A. Laboratory Scale Microgrid Platform

The overall architecture of the constructed microgrid platform is shown in Fig.4, which consists of four essential modules including measurement & monitoring module (MMM), data acquisition module (DAM), computation module (CM) and real-time control module (RCM). A detailed description about this microgrid platform can be referred to our previous work [37].

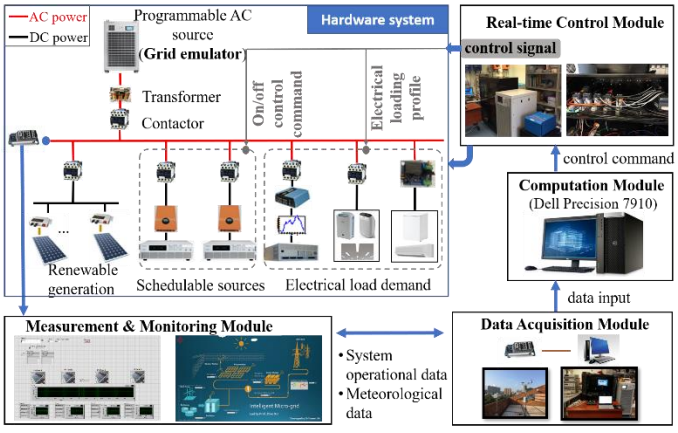

Fig.4 Modular architecture of the microgrid platform

This PHIL platform is a laboratory-scale AC microgrid with total power capacity of 6kW, which comprises of renewable generators (including actual solar PV generation and emulation for both PV and wind generation), schedulable units (emulated by programmable DC sources connecting to DC-AC converters), programmable load and actual load. The electrical properties of each unit are summarized in Table I.

As shown in Fig.4, the normal operation of this platform relies on the synergy among all interactive modules in real time. The MMM senses the system operational status by leveraging

NI measurement devices. The real-time monitoring system is developed in LabVIEW. The DAM is capable of storing real-time measurement data at the rate of 20k samples/s. The stored data can be timely called and processed by the CM for online optimization. Specific energy scheduling methods can be invoked in CM, through which the control commands can be produced periodically and sent to RCM. In RCM, the controllers run in real time for all system components while the scheduling cycles can be intentionally scaled down to a certain extent according to the actual needs.

TABLE I ELECTRICAL PROPERTIES OF EACH SYSTEM COMPONENT

System component	Number of units	Electrical properties
Solar PV generator	4	250W_P monocrystalline silicon panel and 280W micro-inverter are utilized
PV and wind emulator	1	Chroma6200H is utilized as programmable source. The power range is set as [0, 1kW]
Grid emulator	1	Chroma61511 is utilized as programmable AC source. The power flow can be bi-directional. Instant power imbalance is complemented by this device.
Schedulable generators	2	Chroma6200H is utilized as programmable source. The power range is set as [0, 2.5kW]
Controllable load	1	Chroma63200 is utilized as programmable load. The power range is set as [0, 6kW]
Actual load	4	Household load: air purifier (200W), mini fridge (300W), dehumidifier (240W), LED lighting (60W)

B. Operation Modes for PHIL Simulations

The communication between the hardware system and all platform modules is established by deploying User Datagram Protocol over ethernet. The whole structure is shown in Fig.5. On top of the communication system, all microgrid components can be timely monitored and controlled via the control center, and operate in an interactive way.

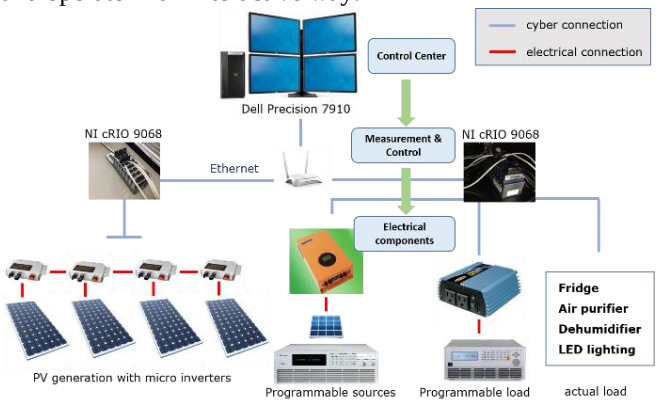

Fig.5 The communication structure of the microgrid platform

The developed microgrid platform can provide flexible operation modes to address the actual testing needs for PHIL simulations.

- *Actual mode*: all system components including actual PV panels, real load and all emulators run and being controlled in real time. Both CM and RCM shall follow the realistic time clock.
- *Scaling mode*: particular generation and loading profiles are generated in the CM and scaled up/down according to a user-defined ratio. In this mode, the control cycles of RCM can be pre-defined.

In both operating modes, system response delay is unavoidable. As shown in Fig.6, control commands should be periodically fed into RCM and trigger actuation of microgrid control. In our microgrid platform, the response delay is normally within 0.2s.

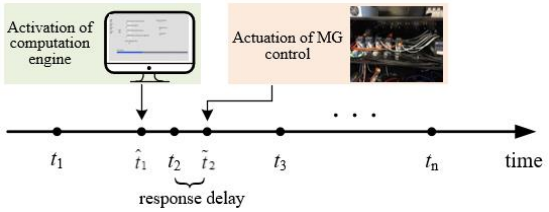

Fig. 6 The schematic diagram of the interaction between CM and RCM

C. PHIL Experiment Settings

The developed PHIL platform serves as a flexible and viable testbed to validate the effectiveness of different scheduling methods. To address specific testing needs, various operating scenarios can be constructed by properly setting and activating each module in due course.

In particular, the following experimental settings are deployed in our study to verify and compare *h*CHASE and MPC under typical operating scenarios.

Testing network structure: the testing network consists of main grid (emulated by the bi-directional AC source), renewable generation, two schedulable units (emulated by programmable sources), and non-/controllable load demand. This testing system is operated in grid-connected mode.

Operation mode: scaling mode is adopted. Real-world historical datasets of renewable generation, load demand and spot price in electricity market are adopted, where the maximum generation power is scaled down to 6kW level and the time-series profiles are scaled down according to the ratio of 15:1. The energy scheduling cycle is set as 1min in the PHIL experiments (i.e. 15min without scaling).

CM settings: specific load demand predictor should be preset in CM and generate lookahead information in each scheduling cycle. MATLAB is utilized as computing engine and interfaced to the whole LabVIEW environment. In consideration of response delay, computation for specific scheduling algorithm should be activated at $\hat{t}_i$ (as shown in Fig.6) to ensure that $t_i - \hat{t}_i$ is adequate to generate the scheduling command for the next cycle.

V. EXPERIMENTAL RESULTS

In this section, *h*CHASE and MPC are comprehensively compared on the constructed PHIL platform.

A. System Operation Data

Real-world historical datasets for renewable generation (i.e. solar PV [38] and wind [39]), load demand [40] and electricity price data [41] are utilized, in which 31 representatives are selected and preset in CM. The selective net loading profiles and electricity price series are shown in Figs.7 and 8.

In the experiment, the parameters of schedulable generators are set in Table II. The settings are reasonably scaled down based on the actual parameters of the large-scale thermal

generators [36].

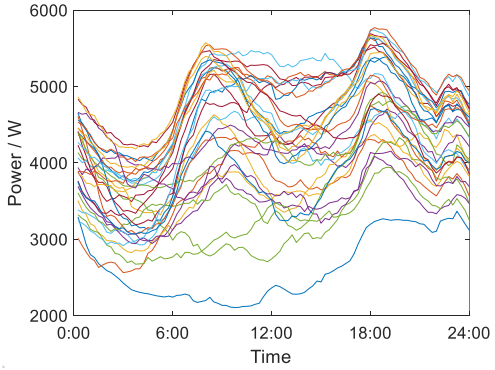

Fig.7 Time-series net-load data of the selective 31 days

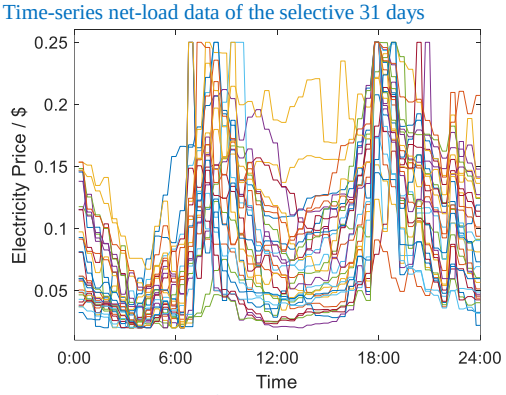

Fig.8 Time-series price data of selective 31 days (the price data is normalized and bounded within [0.02$/kWh,0.25$/kWh])

TABLE II PARAMETER SETTINGS FOR SCHEDULABLE GENERATORS

	$P^{\max}$ (kW)	c^{start} ($)	c^{incr} ($/kWh)	c^{sunk} ($)
G1	2.4	0.57	0.12	0.056
G2	1.8	0.41	0.15	0.04

In our study, LSTM [42], entropy-based DNNE [43] and ELM [44] are utilized as short-term netload predictors. The overall forecasting performance of these three methods is summarized in Table III.

TABLE III FORECASTING PERFORMANCE ON THE GIVEN NETLOAD DATA

	MAPE							
	σ=0	σ=1	σ=2	σ=3	σ=4	σ=5	σ=6	σ=7
LSTM	0.113	0.123	0.157	0.195	0.232	0.273	0.319	0.371
DNNE	0.197	0.212	0.244	0.282	0.314	0.357	0.389	0.432
ELM	0.264	0.276	0.297	0.322	0.347	0.378	0.409	0.440

The forecasting accuracy is generally case-dependent. Based on the forecasting results reported in Table III, it is revealed that the linear approximation utilized in (29) is effective to a certain extent.

B. Theoretical Limits of Competitive Ratio of hCHASE

Given the above microgrid operation data, the theoretical limits of competitive ratio of the proposed scheduling regime are explicitly evaluated according to Theorem 2. The evaluation time frame is set within a particular day. It is intended to compare the change of competitive ratio confronting with different loading peak, price fluctuation and forecasting errors. The evaluation results are reported in Tables IV-VI.

As reported in Tables IV-VI, it is obvious that the upper limits of competitive ratio (i.e. CR_{max}) grows along with the increase of lookahead window. In presence of forecasting information of the future states, the forecasting accuracy plays a key role to affect CR_{max}. As the forecasting accuracy increases, CR_{max} can be considerably decreased. In confronting with large fluctuation of electricity price in comparison with the incremental cost of the local generators (i.e. $\lambda_{\min}^{up} - \lambda_{\min}^{dw}$), *h*CHASE surprisingly exhibits robustness with smaller CR_{max}. Meanwhile, a large loading peak within a day can lead to a relatively large CR_{max}.

TABLE IV THEORETICAL LIMITS OF COMPETITIVE RATIO (WITH LSTM)

σ	G1: $\lambda_{\min}^{up} - \lambda_{\min}^{dw} = 0.053$ G2: $\lambda_{\min}^{up} - \lambda_{\min}^{dw} = 0.042$		G1: $\lambda_{\min}^{up} - \lambda_{\min}^{dw} = 0.047$ G2: $\lambda_{\min}^{up} - \lambda_{\min}^{dw} = 0.039$	
	$P_{load}^{\max} = 5.56kW$	$P_{load}^{\max} = 4.12kW$	$P_{load}^{\max} = 5.56kW$	$P_{load}^{\max} = 4.12kW$
0	CR_{max}=1.6861	CR_{max}=1.6234	CR_{max}=1.6893	CR_{max}=1.6256
1	CR_{max}=1.7195	CR_{max}=1.6606	CR_{max}=1.7257	CR_{max}=1.6647
2	CR_{max}=1.7570	CR_{max}=1.7004	CR_{max}=1.7656	CR_{max}=1.7062
3	CR_{max}=1.7983	CR_{max}=1.7428	CR_{max}=1.8091	CR_{max}=1.7500
4	CR_{max}=1.8435	CR_{max}=1.7879	CR_{max}=1.8561	CR_{max}=1.7962
5	CR_{max}=1.8927	CR_{max}=1.8355	CR_{max}=1.9067	CR_{max}=1.8448
6	CR_{max}=1.9458	CR_{max}=1.8857	CR_{max}=1.9609	CR_{max}=1.8957
7	CR_{max}=2.0028	CR_{max}=1.9385	CR_{max}=2.0186	CR_{max}=1.9490

TABLE V THEORETICAL LIMITS OF COMPETITIVE RATIO (WITH DNNE)

σ	G1: $\lambda_{\min}^{up} - \lambda_{\min}^{dw} = 0.053$ G2: $\lambda_{\min}^{up} - \lambda_{\min}^{dw} = 0.042$		G1: $\lambda_{\min}^{up} - \lambda_{\min}^{dw} = 0.047$ G2: $\lambda_{\min}^{up} - \lambda_{\min}^{dw} = 0.039$	
	$P_{load}^{\max} = 5.56kW$	$P_{load}^{\max} = 4.12kW$	$P_{load}^{\max} = 5.56kW$	$P_{load}^{\max} = 4.12kW$
0	CR_{max}=1.6861	CR_{max}=1.6234	CR_{max}=1.6893	CR_{max}=1.6256
1	CR_{max}=1.7225	CR_{max}=1.6626	CR_{max}=1.7283	CR_{max}=1.6665
2	CR_{max}=1.7657	CR_{max}=1.7062	CR_{max}=1.7735	CR_{max}=1.7114
3	CR_{max}=1.8158	CR_{max}=1.7545	CR_{max}=1.8249	CR_{max}=1.7605
4	CR_{max}=1.8727	CR_{max}=1.8072	CR_{max}=1.8825	CR_{max}=1.8138
5	CR_{max}=1.9364	CR_{max}=1.8645	CR_{max}=1.9463	CR_{max}=1.8711
6	CR_{max}=2.0070	CR_{max}=1.9264	CR_{max}=2.0163	CR_{max}=1.9325
7	CR_{max}=2.0844	CR_{max}=1.9927	CR_{max}=2.0925	CR_{max}=1.9981

TABLE VI THEORETICAL LIMITS OF COMPETITIVE RATIO (WITH ELM)

σ	G1: $\lambda_{\min}^{up} - \lambda_{\min}^{dw} = 0.053$ G2: $\lambda_{\min}^{up} - \lambda_{\min}^{dw} = 0.042$		G1: $\lambda_{\min}^{up} - \lambda_{\min}^{dw} = 0.047$ G2: $\lambda_{\min}^{up} - \lambda_{\min}^{dw} = 0.039$	
	$P_{load}^{\max} = 5.56kW$	$P_{load}^{\max} = 4.12kW$	$P_{load}^{\max} = 5.56kW$	$P_{load}^{\max} = 4.12kW$
0	CR_{max}=1.6861	CR_{max}=1.6234	CR_{max}=1.6893	CR_{max}=1.6256
1	CR_{max}=1.7248	CR_{max}=1.6641	CR_{max}=1.7304	CR_{max}=1.6679
2	CR_{max}=1.7727	CR_{max}=1.7109	CR_{max}=1.7799	CR_{max}=1.7156
3	CR_{max}=1.8297	CR_{max}=1.7637	CR_{max}=1.8376	CR_{max}=1.7689
4	CR_{max}=1.8959	CR_{max}=1.8227	CR_{max}=1.9036	CR_{max}=1.8278
5	CR_{max}=1.9713	CR_{max}=1.8877	CR_{max}=1.9779	CR_{max}=1.8921
6	CR_{max}=2.0558	CR_{max}=1.9588	CR_{max}=2.0606	CR_{max}=1.9619
7	CR_{max}=2.1495	CR_{max}=2.0360	CR_{max}=2.1515	CR_{max}=2.0373

The results discussed above are all about the theoretical limits, which can serve as performance guarantee to justify whether *h*CHASE is viable to provide satisfactory scheduling solutions under a specific scenario. Overall, it can be seen that *h*CHASE is theoretically robust to spot price fluctuations.

In the following subsection, the robustness of *h*CHASE and MPC toward future uncertainty will be evaluated through PHIL simulations.

C. Scheduling Results of hCHASE, MPC and PD

According to the experimental settings in Section IV, PHIL simulations are carried out for the selective 31 days based on different lookahead information. The scheduling profiles of some typical days are shown in Figs.9-11. The comparative scheduling results are reported in Tables VII-IX.

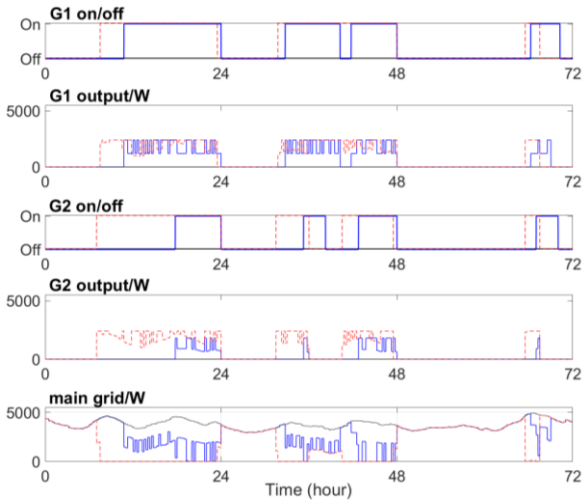

Fig. 9 Energy scheduling profiles on days 10, 11 and 12 (blue line: *h*CHASE; black line: MPC; red dash line: PD; lookahead window: 15min; netload predictor: LSTM, CR_{hCHASE}=1.0901, CR_{MPC}=1.1703).

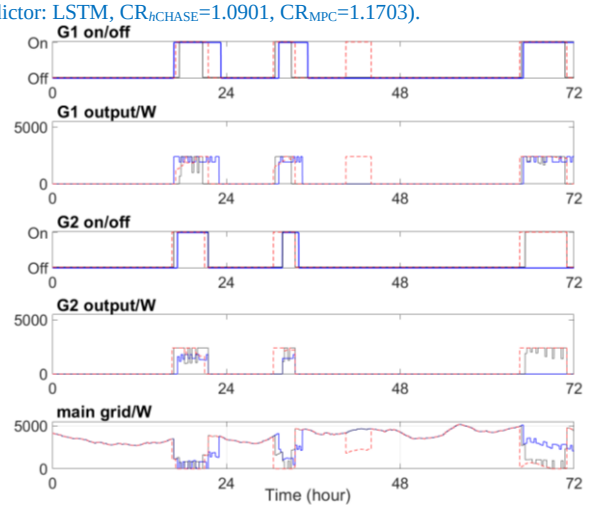

Fig. 10 Energy scheduling profiles on days 5, 6 and 7 (blue line: *h*CHASE; black line: MPC; red dash line: PD; lookahead window: 90min; netload predictor: LSTM, CR_{hCHASE}=1.0732, CR_{MPC}=1.0720)

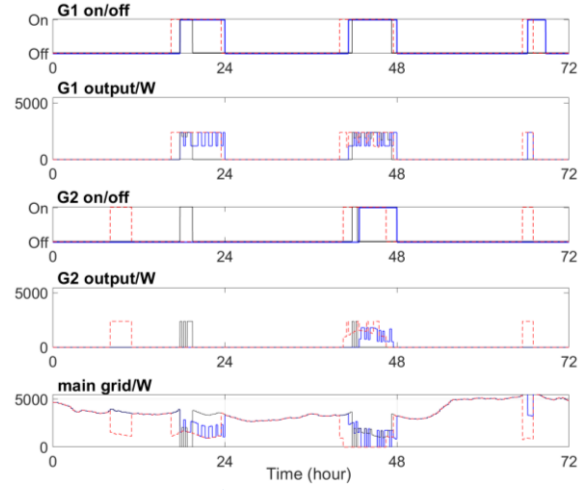

Fig. 11 Energy scheduling profiles on days 25, 26 and 27 (blue line: *h*CHASE; black line: MPC; red dash line: PD; lookahead window: 60min; netload predictor: ELM, CR_{hCHASE}=1.0874, CR_{MPC}=1.0941)

Figs.9-11 present the scheduling profiles of *h*CHASE, MPC and PD under three typical scenarios: i.e. i) limited accurate forecasting information is provided (as shown in Fig. 9); ii) the lookahead window is sufficiently long and the forecasting accuracy is high (as shown in Fig. 10); and iii) the lookahead window is sufficiently long yet the forecasting accuracy is low (as shown in Fig. 11). In Fig.9, the on/off scheduling actions of *h*CHASE closely lag behind the optimal solutions yielded by PD, while MPC fails to turn on the local generators in due course. In case that the lookahead window is sufficiently long for MPC while the forecasting information is less accurate, *h*CHASE still exhibits better performance than MPC as shown in Fig. 11. It can be seen that the scheduling solutions obtained by *h*CHASE and PD are mostly overlapped, while MPC produces several opposite schedules. Meanwhile, the obtained CR_{hCHASE} is less than CR_{MPC} under cases i and iii, which implies that *h*CHASE based scheduling regime is much robust to future uncertainties and outperforms MPC. Given that the lookahead window size can make MPC effective and the forecasting accuracy is high, as shown in Fig.10, MPC provides better scheduling performance than *h*CHASE.

TABLE VII EXPERIMENTAL RESULTS (PREDICTOR: LSTM)

σ	Competitive Ratio (in average of 31 days)	
	*h*CHASE	MPC
0	1.0910	1.1676
1	1.0887	1.1676
2	1.0812	1.1676
3	1.0786	1.1159
4	1.0781	1.0903
5	1.0742	1.0755
6	1.0727	1.0720
7	1.0793	1.0709

TABLE VIII EXPERIMENTAL RESULTS (PREDICTOR: DNNE)

σ	Competitive Ratio (in average of 31 days)	
	*h*CHASE	MPC
0	1.0910	1.1676
1	1.0895	1.1676
2	1.0862	1.1676
3	1.0814	1.1201
4	1.0801	1.0920
5	1.0787	1.0843
6	1.0789	1.0801
7	1.0818	1.0827

TABLE IX EXPERIMENTAL RESULTS (PREDICTOR: ELM)

σ	Competitive Ratio (in average of 31 days)	
	*h*CHASE	MPC
0	1.0910	1.1676
1	1.0901	1.1676
2	1.0888	1.1676
3	1.0872	1.1274
4	1.0874	1.0940
5	1.0887	1.0905
6	1.0892	1.0935
7	1.0896	1.0932

In Tables VII-IX, competitive ratios obtained by *h*CHASE and MPC with different levels of future uncertainties are comprehensively compared. In this paper, we measure the uncertainties by using lookahead time steps and forecasting accuracy. As discussed in Section II, due to the algorithmic mechanisms of these two methods, MPC is strongly prediction-dependent while *h*CHASE is prediction-oblivious. Simulation results reported in Tables VII-IX are consistent with this argument.

Specifically, in Table VII, LSTM provides high forecasting accuracy. It is shown that CRs of *h*CHASE exhibit monotonic decrease given limited forecasting information (i.e. when σ is

less than 6), which implies that limited accurate forecasting information can also facilitate the overall performance of *h*CHASE. The same situations occur in Tables VIII and IX, while provided σ less than 5 and 3, respectively. This is reasonable since much inaccurate future information may negatively lead to misleading decisions. As comparison, MPC becomes less effective given limited future information. In Tables VII-IX, it is obvious that most of the obtained CRs by MPC are much greater than the ones by *h*CHASE. Visually, it is shown that a large mismatch exists between the solutions of MPC and PD in Fig. 9. Overall, one can safely conclude that *h*CHASE is much robust to future uncertainty as compared to MPC.

In considering the forecasting accuracy as the only viable factor, it can be seen that the obtained CRs in Tables VII-IX are dramatically decreased along with the increase of forecasting accuracy. This is consistent with the trend of the derived theoretical limits. Moreover, it is found that even if high uncertainty gets involved (i.e. accurate future information is limited), *h*CHASE still remains practically effective with small CRs as compared to its theoretical limits.

In case that future information is sufficiently provided with high forecasting accuracy (e.g. in Table VII, σ>6), MPC gives rise to smaller CRs than *h*CHASE does. Nevertheless, such cases are unrepresentative in small-scale microgrids since accurately forecasting short-term netload in small-scale system still remains challenging.

VI. Conclusion

To tackle the uncertainty involved energy scheduling problem in microgrid, this paper proposes a novel retrospect-inspired *h*CHASE scheduling regime, of which the practical implementation relies on zero or little forecasting information. As compared to the basic CHASE algorithm, *h*CHASE features the ability of handling heterogeneity of multiple generators. To verify the effectiveness of *h*CHASE, this paper firstly provides the rigorous proofs for its performance guarantee subject to certain degree of forecasting accuracy. Secondly, to fill in the gap between theoretical models and practical implementation, this paper contributes a design of laboratory-scale microgrid platform for PHIL simulation. On the constructed PHIL platform, *h*CHASE and MPC are comprehensively tested and compared. The experimental results are consistent with the theoretical analyses. Furthermore, it is found that the proposed scheduling regime based on *h*CHASE is robust to high operational uncertainty. To further extend the applicability of the proposed *h*CHASE, our future work will focus on stand-alone microgrid, in which the energy storage system will be properly and economically scheduled in a heuristic manner and power balance can be maintained in real-time.

References

[1] M. Mao, P. Jin, L. Chang, and H. Xu, "Economic analysis and optimal design on microgrids with SS-PVs for industries," *IEEE Transactions on Sustainable Energy*, vol. 5, no. 4, pp. 1328-1336, 2014.

[2] A. Ehsan, M. Cheng, and Q. Yang, "Scenario-based planning of active distribution systems under uncertainties of renewable generation and electricity demand," *CSEE Journal of Power and Energy Systems*, vol. 5, no. 1, pp. 56-62, 2019.

[3] F. Farzan, M. A. Jafari, R. Masiello, and Y. Lu, "Toward optimal day-ahead scheduling and operation control of microgrids under uncertainty," *IEEE Transactions on Smart Grid*, vol. 6, no. 2, pp. 499-507, 2015.

[4] A. Parisio and L. Glielmo, "A mixed integer linear formulation for microgrid economic scheduling," in *2011 IEEE International Conference on Smart Grid Communications (SmartGridComm)*, 2011: IEEE, pp. 505-510.

[5] R. Mallol-Poyato, S. Salcedo-Sanz, S. Jiménez-Fernández, and P. Díaz-Villar, "Optimal discharge scheduling of energy storage systems in MicroGrids based on hyper-heuristics," *Renewable Energy*, vol. 83, pp. 13-24, 2015.

[6] W. Su, J. Wang, and J. Roh, "Stochastic energy scheduling in microgrids with intermittent renewable energy resources," *IEEE Transactions on Smart Grid*, vol. 5, no. 4, pp. 1876-1883, 2014.

[7] T. Niknam, R. Azizipanah-Abarghooee, and M. R. Narimani, "An efficient scenario-based stochastic programming framework for multi-objective optimal micro-grid operation," *Applied Energy*, vol. 99, pp. 455-470, 2012.

[8] M. Alipour, B. Mohammadi-Ivatloo, and K. Zare, "Stochastic scheduling of renewable and CHP-based microgrids," *IEEE Transactions on Industrial Informatics*, vol. 11, no. 5, pp. 1049-1058, 2015.

[9] F. Conte, S. Massucco, M. Saviozzi, and F. Silvestro, "A stochastic optimization method for planning and real-time control of integrated pv-storage systems: Design and experimental validation," *IEEE Transactions on Sustainable Energy*, vol. 9, no. 3, pp. 1188-1197, 2018.

[10] P. Kou, D. Liang, and L. Gao, "Stochastic energy scheduling in microgrids considering the uncertainties in both supply and demand," *IEEE Systems Journal*, vol. 12, no. 3, pp. 2589-2600, 2018.

[11] J. D. Lara, D. E. Olivares, and C. A. Cañizares, "Robust energy management of isolated microgrids," *IEEE Systems Journal*, no. 99, pp. 1-12, 2018.

[12] R. Gupta and N. K. Gupta, "A robust optimization based approach for microgrid operation in deregulated environment," *Energy Conversion and Management*, vol. 93, pp. 121-131, 2015.

[13] Y. Zhang, N. Gatsis, and G. B. Giannakis, "Robust energy management for microgrids with high-penetration renewables," *IEEE Transactions on Sustainable Energy*, vol. 4, no. 4, pp. 944-953, 2013.

[14] R. Jiang, J. Wang, and Y. Guan, "Robust unit commitment with wind power and pumped storage hydro," *IEEE Transactions on Power Systems*, vol. 27, no. 2, pp. 800-810, 2012.

[15] D. Sáez, F. Ávila, D. Olivares, C. Cañizares, and L. Marín, "Fuzzy prediction interval models for forecasting renewable resources and loads in microgrids," *IEEE Transactions on Smart Grid*, vol. 6, no. 2, pp. 548-556, 2015.

[16] A. Baziar and A. Kavousi-Fard, "Considering uncertainty in the optimal energy management of renewable micro-grids including storage devices," *Renewable Energy*, vol. 59, pp. 158-166, 2013.

[17] E. C. Umeozor and M. Trifkovic, "Operational scheduling of microgrids via parametric programming," *Applied energy*, vol. 180, pp. 672-681, 2016.

[18] B. Zhao, Y. Shi, X. Dong, W. Luan, and J. Bornemann, "Short-term operation scheduling in renewable-powered microgrids: A duality-based approach," *IEEE Transactions on Sustainable Energy*, vol. 5, no. 1, pp. 209-217, 2014.

[19] S. Mohammadi, S. Soleymani, and B. Mozafari, "Scenario-based stochastic operation management of microgrid including wind, photovoltaic, micro-turbine, fuel cell and energy storage devices," *International Journal of Electrical Power & Energy Systems*, vol. 54, pp. 525-535, 2014.

[20] F. Garcia-Torres and C. Bordons, "Optimal economical schedule of hydrogen-based microgrids with hybrid storage using model predictive control," *IEEE Transactions on Industrial Electronics*, vol. 62, no. 8, pp. 5195-5207, 2015.

[21] W. Gu, Z. Wang, Z. Wu, Z. Luo, Y. Tang, and J. Wang, "An online optimal dispatch schedule for CCHP microgrids based on model predictive control," *IEEE transactions on smart grid*, vol. 8, no. 5, pp. 2332-2342, 2017.

[22] M. P. Marietta, M. Graells, and J. M. Guerrero, "A rolling horizon rescheduling strategy for flexible energy in a microgrid," in *2014 IEEE International Energy Conference (ENERGYCON)*, 2014: IEEE, pp. 1297-1303.

[23] R. Palma-Behnke *et al.*, "A microgrid energy management system based on the rolling horizon strategy," *IEEE Transactions on smart grid*, vol. 4, no. 2, pp. 996-1006, 2013.

[24] N. Holjevac, T. Capuder, N. Zhang, I. Kuzle, and C. Kang, "Corrective receding horizon scheduling of flexible distributed multi-energy microgrids," *Applied Energy*, vol. 207, pp. 176-194, 2017.

[25] B. Gisin, Q. Gu, J. V. Mitsche, S. Tam, and H. Chen, "“Perfect Dispatch”-as the measure of PJM real time grid operational performance," in *IEEE PES General Meeting*, 2010: IEEE, pp. 1-8.

[26] L. Lu, J. Tu, C.-K. Chau, M. Chen, and X. Lin, *Online energy generation scheduling for microgrids with intermittent energy sources and co-generation* (no. 1). ACM, 2013.

[27] L. Lu, J. Tu, C.-K. Chau, M. Chen, Z. Xu, and X. Lin, "Towards real-time energy generation scheduling in microgrids with performance guarantee," in *Power and Energy Society General Meeting (PES), 2013 IEEE*, 2013: IEEE, pp. 1-5.

[28] W.-J. Ma, J. Wang, V. Gupta, and C. Chen, "Distributed energy management for networked microgrids using online ADMM with regret," *IEEE Transactions on Smart Grid*, vol. 9, no. 2, pp. 847-856, 2018.

[29] J. Wang, Y. Song, W. Li, J. Guo, and A. Monti, "Development of a universal platform for hardware in-the-loop testing of microgrids," *IEEE Transactions on Industrial Informatics*, vol. 10, no. 4, pp. 2154-2165, 2014.

[30] A. C. Luna, L. Meng, N. L. Diaz, M. Graells, J. C. Vasquez, and J. M. Guerrero, "Online energy management systems for microgrids: experimental validation and assessment framework," *IEEE Transactions on Power Electronics*, vol. 33, no. 3, pp. 2201-2215, 2018.

[31] J.-H. Jeon *et al.*, "Development of hardware in-the-loop simulation system for testing operation and control functions of microgrid," *IEEE Transactions on Power Electronics*, vol. 25, no. 12, pp. 2919-2929, 2010.

[32] F. Huerta, R. L. Tello, and M. Prodanovic, "Real-time power-hardware-in-the-loop implementation of variable-speed wind turbines," *IEEE Transactions on Industrial Electronics*, vol. 64, no. 3, pp. 1893-1904, 2017.

[33] T. Roinila *et al.*, "Hardware-in-the-Loop Methods for Real-Time Frequency-Response Measurements of on-Board Power Distribution Systems," *IEEE Transactions on Industrial Electronics*, vol. 66, no. 7, pp. 5769-5777, 2019.

[34] M. H. Hajiesmaili, C.-K. Chau, M. Chen, and L. Huang, "Online microgrid energy generation scheduling revisited: The benefits of randomization and interval prediction," in *Proceedings of the Seventh International Conference on Future Energy Systems*, 2016: ACM, p. 1.

[35] J. Youwei, L. Xue, C. S. Lai, X. Zhao, and C. Minghua, "A retroactive approach to microgrid real-time scheduling in quest of perfect dispatch solution," *Journal of Modern Power Systems and Clean Energy*, vol. 7, no. 6, pp. 1608-1618, 2019.

[36] W.-P. Schill, M. Pahle, and C. Gambardella, "Start-up costs of thermal power plants in markets with increasing shares of variable renewable generation," *Nature Energy*, vol. 2, no. 6, p. 17050, 2017.

[37] Y. Jia, Y. He, X. Lyu, S. Chai, Z. Xu, and M. Chen, "Hardware-in-the-loop implementation of residential intelligent microgrid," in *2018 IEEE Power & Energy Society General Meeting (PESGM)*, 2018: IEEE, pp. 1-5.

[38] Solar Power Generation in Belgian Power Grid, online accessible: http://www.elia.be/en/grid-data/

[39] NREL Wind Data and Tools, online accessible: https://www.nrel.gov/wind/data-tools.html

[40] Load and Load Forecasts data in Belgian Grid, online accessible: http://www.elia.be/en/grid-data/Load-and-Load-Forecasts

[41] Electricity Price and Demand, AEMO, online accessible: http://www.aemo.com.au/Electricity/National-Electricity-Market-NEM/Data-dashboard

[42] W. Kong, Z. Y. Dong, Y. Jia, D. J. Hill, Y. Xu, and Y. Zhang, "Short-term residential load forecasting based on LSTM recurrent neural network," *IEEE Transactions on Smart Grid*, 2017.

[43] Y. Jia, Z. Xu, L. L. Lai, and K. P. Wong, "Risk-based power system security analysis considering cascading outages," *IEEE Transactions on Industrial Informatics*, vol. 12, no. 2, pp. 872-882, 2016.

[44] G.-B. Huang, Q.-Y. Zhu, and C.-K. Siew, "Extreme learning machine: theory and applications," *Neurocomputing*, vol. 70, no. 1-3, pp. 489-501, 2006.